IEEE Access
Multidisciplinary ⋮ Rapid Review ⋮ Open Access Journal

Received 22 April 2023, accepted 22 May 2023, date of publication 24 May 2023, date of current version 6 June 2023.

Digital Object Identifier 10.1109/ACCESS.2023.3279712

METHODS

Force and Sound Data Fusion for Enhanced Tap Testing Scanning of Composites

ALASTAIR POOLE [1,2] AND NATHAN HARTLEY [2]
[1]Centre of Ultrasonic Engineering, University of Strathclyde, G1 1XQ Glasgow, U.K.
[2]The Welding Institute (TWI), SA13 1SB Port Talbot, U.K.

Corresponding author: Alastair Poole (alastair.poole@strath.ac.uk)

This work was supported in part by the Engineering and Physical Sciences Research Council (EPSRC) as part of an ICASE Ph.D. Studentship under Grant S513908/1, and in part by the Welsh European Funding Office (WEFO) using European Regional Development Funds (ERDF).

ABSTRACT Coin or hammer tap testing is one of the oldest methods of NDT inspection. Inspection techniques originated with human operators observing the tonal change of the audible sound produced by striking were later automated with use of mechanical instruments that measured surface stiffness from the contact time of the striker. Numerous applications have evolved from this technique, from predicting rock falls to defect detection and identification in composite structures. Since operator applied tap testing requires extensive training and knowledge of the part's structure to accurately locate defects, it is widely regarded as a subjective method and does not allow for digitised recording of results or validation against reference standards. In addition, this type of tap testing is generally confined to simple structural materials such as thin skin composites with foam or honeycomb cores, where defects can easily be identified. More complex structures with varying thicknesses present a much greater challenge for this method, as defects may have a similar response signal to thinner, non-defective regions, so neither force nor sonic data can differentiate between the two. This article seeks to introduce a novel analysis technique, applying the principle of resonant membranes to global and local frequency perspectives to generate two functions. The first sharpens tap testing images from the sonic and force responses returning greater clarity when observing the underlying structure, the second creating a local ranking of defect positions allowing an automatic highlighting of regions of high depth flux. The outcome is a process that enables operators to identify disbonds within an unknown composite structure with greater precision than either force or sound approaches on their own in lieu of prior information of defect, surface, or global resonance modes. The developed technique is suitable for application with a robotic platform to unknown curved composites surfaces since future developments will aim to achieve robotised TT deployment. The algorithm is validated within a laboratory environment on a physical reference sample, representative of an RNLI Severn class lifeboat hull, imitating a dry-dock inspection scenario.

INDEX TERMS Tap testing, force/sound data fusion, thick composite inspection.

I. INTRODUCTION

Several challenges are faced when inspecting the integrity of Glass Fibre Reinforced Plastics (GFRP) boat hulls of varying structure and age within a dry dock environment. Traditional techniques such as Ultrasound are often unable to penetrate the composite and its paint coating with an acceptable signal to noise ratio. Radiographic scans, though accurate, pose a health risk to others within the dry-dock, resulting in large down-times for other work. The authors have turned to traditional Tap-Testing (TT) due to its success in other similar materials. Traditionally, TT requires a highly trained operator equipped with foreknowledge of the structure to discriminate changes in thickness from defects. Use of legacy hulls and hulls without detailed digital twins complicate the process, since variations in the hull's structure may be confused with

The associate editor coordinating the review of this manuscript and approving it for publication was Ravibabu Mulaveesala.

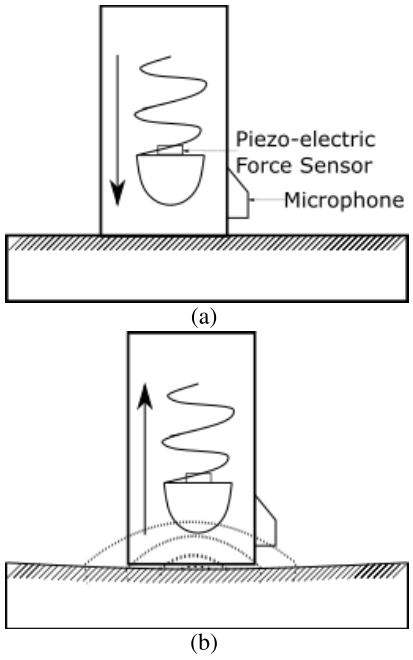

FIGURE 1. Instrumented Tap-Testing equipment set-up. 1a depicts the Piezo-electric force sensor and microphone mounted to the instrumented tap testing housing, where the mass accelerates towards and strikes the surface. 1b, the resultant flexure of surface results in a pressure upon the mass while it is in contact with the part that is measured by the Piezo-electric sensor, and sound emitted by surface resonance that is collected by the microphone.

defects, complex sub-structures have traditionally required other NDT techniques due to the relative inaccuracy of the TT method. Exterior damage can easily be assessed with visual inspection of the outer hull, and so only internal or sub-surface issues need to be considered.

Non-instrumented deployment of TT required a human operator to impact a surface with either a coin or hammer and resultant changes in the sound used to locate potential defects. The sonic response as a result of surface vibrations is also found to be recorded through the force-time history of the impact with near-surface defects. This was later developed into an instrumented tapping method, whereby a mass would strike a surface, and either a Piezo-electric piece in rigid contact with the mass would monitor the impact force history, or a microphone would be used to listen to the resultant surface vibrations in order to detect defects, a graphical set-up of which is shown in Fig: 1. An example of the measured impact force and sound responses are shown in Fig: 2.

Building on previous impact modelling [1], the impact is modelled by [2] as a parallel two-spring system, of contact and defect stiffness. The natural harmonic frequency's dependence on defect stiffness value k and tapping-implement mass m correlates the time of impact τ to probable presence of a defect related to the stiffness;

$$\tau = \pi\sqrt{\frac{m}{k}}, \tag{1}$$

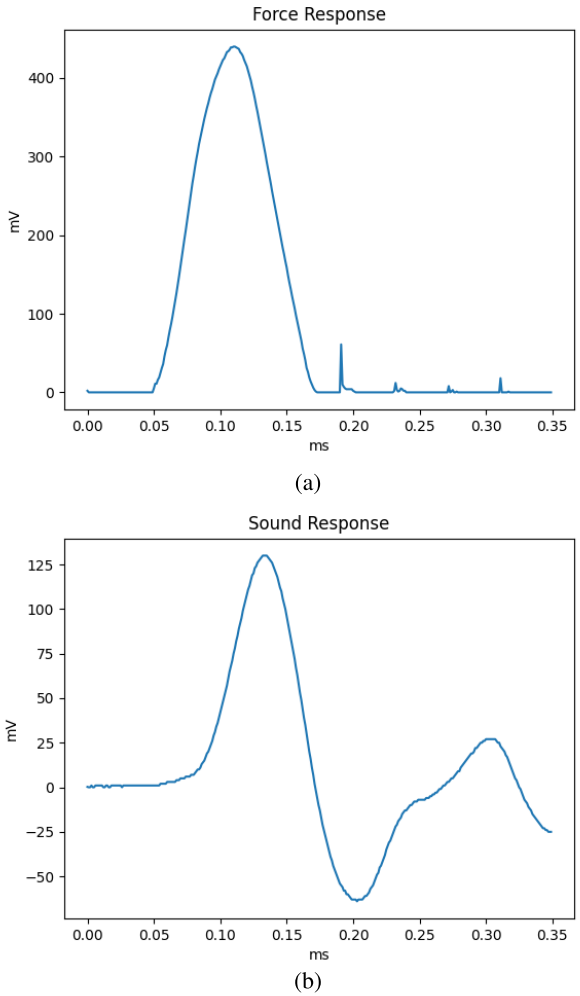

FIGURE 2. Force and sound response examples taken with an EVOTIS tap testing device. Both Piezo force and microphone sound sensors collect in units of *mV*. 2a illustrates the force felt by the instrumented tap testing device during contact of the tapping element with the part, a semi-sinusoidal wave modelled as a dual-spring model introduced in Eq: 1. The force induces surface modes of oscillation that result in audible noise heard by the tap testing device's microphone, shown in 2b.

where thinner/defective surface regions have a reduced stiffness coefficient. Force-time used as a proxy for audible acoustic frequency is applied to highly critical composite testing procedures due to its reliability and repeatability for certain materials [3], [4], [5], though only accurate to limited depths. The information within the force-time history has inspired Artificial-Intelligence (AI) approaches to defect classification as well as identification in aeronautical components [6]. Direct measurement of local stiffness effectively indicates near-surface defects such as voids but provides less accurate results for measurements within the material's bulk.

Audible measurements can provide greater information of defects at depth within a part. Utilising audible measurements, [7] applied previous work in membrane resonance NDT [8] to determine the detectability of defects using the induced sound with respect to defect width and depth. This detectability index assumes the local membrane resonance

directly around the defect is significant within the audible signal if the initial impact contains the defective regions' resonant frequencies, underpinning the theoretical aspects of: [8]. This work also produced a frequency-independent cost function for assessing structural integrity. The signal energy of the resultant sound is used to differentiate local structural depths. The energy E of the signal $s(t)$ heard by the microphone within a discrete time domain $t \in [0, T]$ is proportional to [9];

$$E = \sum_{t=0}^{T} |s(t)|^2. \tag{2}$$

Thicker surfaces are less deformed than thinner parts by equal forces, resulting in a duller, equivalently a less energetic tonal response enabling the detection of surface depth. Importantly, this analysis demonstrates that a low-mass striker induces a wide band of frequencies in the material, allowing imaging in structures of varying thicknesses. The results are however noisy, as can be seen in Section: IV, an issue when the structure is not well-known, potentially leading to an operator highlighting false-positives for defects within the hull.

Modelling for steel structures has demonstrated that defects' local resonance does dominate the signal [10]. Despite this, the key study of TT sonic/force analysis methods applied to thick composites by [11] shows that the vibrational modes of the surface locally and globally need to be considered in order to build an accurate defect map for thick composites. The additional outcome of this study is the determination that force and sound combined can provide more information than either on their own, though without a suitable fusion method.

Several other approaches have sought to fuse or use both force and sound data to provide more information than either individually. The investigation of [12] found that the free-vibration sound (after the hammer's contact period) provides substantial information of bulk defects. Despite this, non-uniform response and propagation of surface vibration frequencies produces irregular results over the surface, highlighting machine learning methods as a necessary method to enhance signal interpretation. The Neural Network approach investigated by [13] found that the fusion of force/sound could provide a 100% true negative rate for non-defective regions, and a high true-positive rate for defects in fibreglass and Balsa wood samples. While this this is a demonstrably successful approach, there are two draw-backs of this approach for this use case. Firstly, the necessity for training data precludes use in this case on-site since a process would preferably be used on multiple boat-hull types with varying thicknesses due to differing specifications and manufacturing processes. Secondly and more significantly, machine learning processes require the defective and non-defective regions have unique depth signatures, which is not the case for the disbonding cases considered. This is illustrated in Fig: 3 where the defect's sonic signature is nearly identical to a non-defective region, due to the part's varying thickness.

Meanwhile, a subsection of papers investigating Force Reconstruction (FR) also study the correlation of force and sound responses. Modelling or measuring the sound produced by an elastic wave within the surface allows the deduction of impact force and location from microphone data collected from multiple positions [14]. While in idealised scenarios such as circular or square plates, resonant modes are derived throughout the literature, for surfaces with either complex shapes or material characteristics, physical models are considered unreliable [15] while prior information approaches provide reliable results [16]. Even then, modal spread due to non-uniform surface features makes prior information incorporation difficult. However, errors in impact estimation caused by irregular mode propagation implies that if the force and relative position of the impact to the microphone is constant, variations in the surface stiffness and depth can be mapped by cross-correlation variations within the frequency domain.

Applying this concept from a parallel field, this paper seeks to introduce a novel approach to TT data processing resulting in smoother and more reliable maps for structural depth imaging than traditional techniques using only the audible response. The second output of this paper is a novel metric function that quantifies and estimates surface non-uniformities as a result of cross correlation of data in the frequency domain. The process is described in Section: II, then experimentally validated in Section: IV. Applicable to naive mapping of surfaces, this method is shown to enable an operator to accurately detect changes, anomalies and discontinuities in regular features of thick composite structures, which may be defects or irregular features such as sensor pockets, limber holes or internal bracketry. The combination of these maps results in a thickness variation map that more accurately represents the structure, and a defect recognition process that selects regions of concern.

II. ENHANCED RESOLUTION IMAGING

Several papers have highlighted the effect of non-local modes on the frequency response of the audible sound, and also the need to separate the two sources of audible response in order to obtain high quality imaging of components. A large portion of TT research has focused on the force-time response alone for this reason, as it is reflective of local modes of excitation only. While sound baffling could be used to shield the microphone from globally resonant modes, this would present significant challenges if robotically deployed as is the goal application of this technology. Rigid baffles would not conform well to parts of varying curvature, preventing isolation of the microphone from global resonant sound sources. Flexible baffles would present an issue for a robot in approaching the part and when covering the surface, causing snagging issues where a human operator would simply rearrange the probe.

Separately, FR approaches such as [17] relate the sound heard at time t and position $\vec{x}$ due to an impact force $F(t)$ at

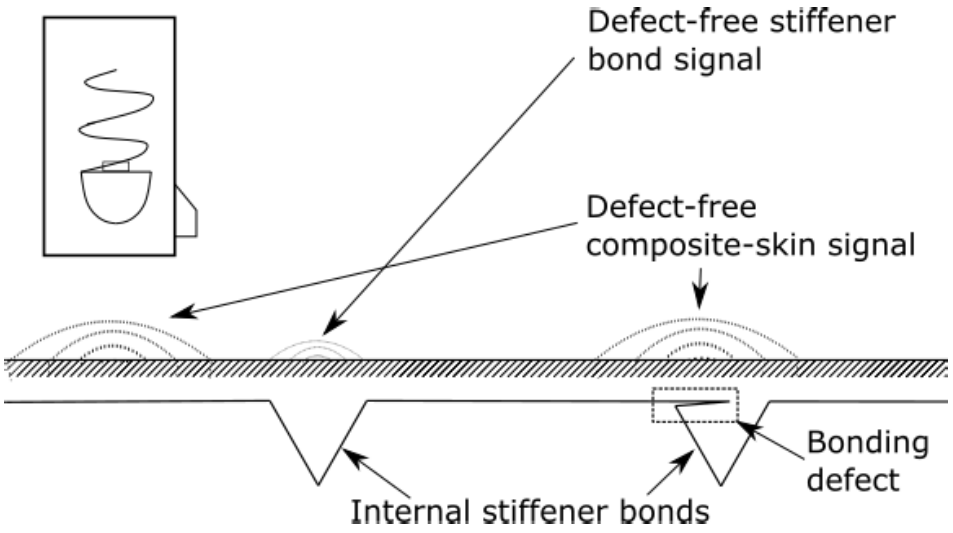

FIGURE 3. Cross-sectional schematic of depth measurement. An cross sectional image of a realistic hull sample is shown later in Fig: 5. While machine-learning methods applied to TT use prior information in order to detect unique outlier sonic or force response signatures to identify defects, for this case the varying depth can result in defect-free classification of defective positions. This issue is highlighted later with TT data in Section: IV.

the global origin by;

$$s(\vec{x}, t) = \int_0^t G(t-\tau, \vec{x})F(\tau)d\tau. \tag{3}$$

where G is the Greens function, propagating surface acceleration within the spatio-temporal domain, since this is directly related to the audible emissions. Analysing the sonic/force responses in the discrete frequency domain, the force/sound frequency kernel H takes a matrix form;

$$H_{i,j} = \frac{s(f_i)\bar{F}(f_j)}{|\bar{F}|^2}, \tag{4}$$

where $H_{i,j}$ is the convolution matrices i^{th} row and j^{th} column entry, and $\bar{F}$ is the complex conjugation of the force-frequency spectrum. Taking a similar approach to [18], we equate the total sound heard by the microphone to a Rayleigh integral over the surface, introducing the new Green's function $\hat{G}$ that relates the initial impact force with the sound emitted from a surface position at a later time. Since, using the Rayleigh integral approach, the sound emitted from an infinitesimal position is proportional to surface acceleration that is in turn related to force propagation. This is an appropriate approach to take. Considering a wave of depth and frequency dependent on position, where $\vec{x} \in R$, the total measured sonic response $\hat{s}$ form the microphone's position $\vec{q}$ in the time domain is;

$$\hat{s}(t) = \int_R \int_0^t \hat{G}\left(t-\tau-\frac{|\vec{x}-\vec{q}|}{c}, \vec{x}\right)\frac{F(\tau)}{|\vec{x}-\vec{q}|}d^m x d\tau. \tag{5}$$

Applying the convolution kernel to the sound heard by a microphone;

$$\hat{s}(f) = \hat{H}F(f), \tag{6}$$

and transforming the components of Eq: 5 individually;

$$\hat{H} = \int_R \hat{H}_x \frac{d^m x}{|\vec{x}-\vec{q}|}. \tag{7}$$

We modify Eq: 2 to only reflect the local modal energies. We decompose $\hat{H}$ into $\hat{H} = \hat{H}^{\parallel} + \hat{H}^{\perp}$, where $\hat{H}^{\parallel}$ and $\hat{H}^{\perp}$ are diagonal and off-diagonal components respectively. The literature of impact response and TT stress the interaction and conversion of locally instrumented forces and their conversion to global and local modalities. Depth of the part is also a key determinant of the surface resonant frequency. Under an idealised system, the matrix $\hat{H}^{\parallel}$ represents the force directly exciting the local fundamental frequencies, that are also shown in the force history measurements. The matrix $\hat{H}^{\perp}$ represents modal conversions to global excitations that differ from local modes due to non-isotropic material properties and the varying depth of the part, converting the initial impact energy to sound energy within a broader set of audible frequency bands. Modelling the interaction of sound and force this way and taking the results of previous studies we infer that the local and global modes are excited by the initial impact, with the local modes representing an expanding elastic surface wave while surface stiffness diffuses the vibration energy towards the lower frequency global modes, seen in Fig: 4. As a result of this model, we expect a monotonic fractional increase in the dominance of off-diagonal elements as the impact energy is transferred to the global modes, given by Eq: 9.

Taking this perspective, the sound energy observed due to excitations of only the local modalities that reflect the local depth values E_ϵ is then reinterpreted from Eq: 2;

$$E_\epsilon = \sum_f |\hat{H}^{\parallel}F(f)|^2, \tag{8}$$

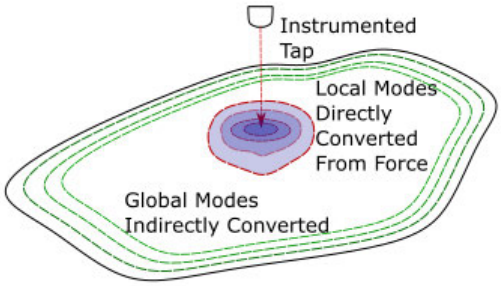

FIGURE 4. An instrumented tap causes material vibrations involving both local and non-local resonant modes. Interactions of the observed force and sound frequencies describes the conversion rate of energy from local to global resonances.

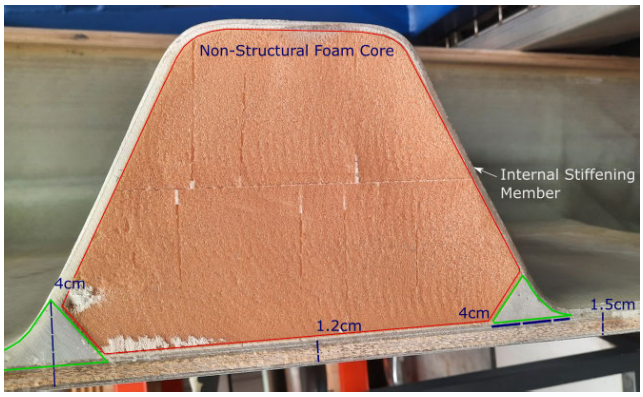

FIGURE 5. Cross section of the part. Primary areas of interest in which disbonding may occur are highlighted in green, the secondary areas are in the outer (lower) composite material. The non-structural foam core is clad in the internal stiffener member that is in turn fastened to the outer composite material with the stiffener bonds (green).

the first novel evaluation function we introduce and call the matrix trace method. Where parts are of uniform or known thickness, methods such as simple frequency spectrum filtering would be an alternative to Eq: 2, since prior knowledge of local resonant frequencies could be ascertained. However in cases where the surface depth is unknown or a calibration model unavailable, prior knowledge cannot be incorporated. In consideration of the use case and future deployments with a robotic system, inclusion of prior knowledge and sound baffles is undesirable.

Accurate local depth measurement allows an operator to identify the hidden structure of thick composites. While other leading studies of TT utilise depth data to identify defects through machine learning methods, this is not applicable when the structure is unknown and of varying depth since a defect can be of the same depth and contain the same force and sonic response as a non-defective region, as exampled by the schematic in Fig: 3. In this case, the rate of change of depth information provides greater clarity of the presence of a defect.

Variations in structure can be measured as a function of the fraction of indirect force to sound conversion. A proportion of the initial resonant impact spectra produced by the tap and observed by the force undergoes modal conversions to non-local modes of vibration. Modal conversion's impact on the acoustic energy distribution through the observed frequency spectra reflects the similarity of the part's local and semi-local depths. Regions with consistent depth in the semi-locality will undergo little if any modal conversion, whereas regions with large depth variations will convert a larger portion of the acoustic energy to modes different to the local spectra. The second novel function is introduced;

$$q(\hat{H}) = \frac{|\hat{H}|_2^2 - |(\hat{H}^{\parallel})|_2^2}{|\hat{H}|_2^2} = \frac{|(\hat{H}^{\perp})|_2^2}{|\hat{H}|_2^2}, \tag{9}$$

where $|*|_2$ is the Frobenius norm. This metric q provides a metric for semi-local depth variations that highlights regions of rapid flux in depth. This is experimentally validated in Section: IV-B.

To provide accurate mapping of surface depth, this paper has introduced the novel function: 8 that considers only local contributions to the sonic response of an instrumented tap, formally seen as exclusive benefit of the force response metric, but also containing the depth data available to the sonic response providing local structural information in greater clarity than the commonly used function Eq: 2. While this function is inspired by research within the domain of FR, it introduces the novel concept of frequency domain separation using impact force information unavailable to FR analyses. This paper has further introduced the novel metric q in Eq: 9, detecting the rate of change of surface depth. Whereas traditional TT methods rely on depth data alone for defect detection, in cases of varying depth or unknown structure the rate of change of depth provides a more informative mapping of defective regions as is shown later in Section: V.

III. LIFEBOAT HULL COMPONENT

Critical defects in this analysis are delaminations of the outer GFRP skin from the internal stiffening members, in particular at the areas where these two components meet as highlighted in green in Fig: 5 to the hull, potentially leading to loss of rigidity and ultimately structural failure. Additional intra-composite delaminations in the outer layer are considered also, as wear and tear can lead to internal damage.

Two artificial defects were created as back-drilled holes of $10cm \times 10cm$ representing these two defect types. These are shown from the back of the part in Fig: 6.

A frontal map showing both defects overlayed on the grid used for guiding scans is shown in Fig: 7.

The depth differentials between each defects and the surrounding hull vary significantly, with defect one's cut through the stiffener creating a depth differential of $3.5cm$, and for defect two, a depth differential of only $1cm$. Using sonic depth imaging metrics, defect one should be significantly easier to identify than defect two due to the greater difference in defect to surface depth values. The break in the stiffener member will still however have a similar signature to the surrounding

FIGURE 6. Artificial defects embedded within the surface. Their dimensions are 10*cm* × 10*cm* since defects below this threshold are not considered critical. Defect one represents a delamination of the stiffener member, cutting through the stiffener and intersecting the non-structural core with a depth of 0.2*cm* from the outside of the hull. A portion of the defect is present under the structural foam, represented by the dotted line. Defect two represents internal tear and wear to the hull's skin with a depth of 0.5*cm* from the outside of the hull. The image is reflected and rotated anti-clockwise by 90° relative to the images produced as a result of scanning later.

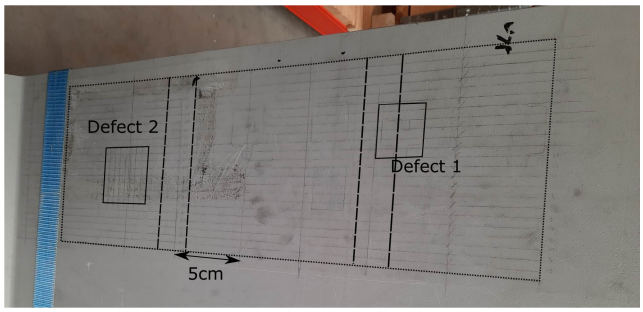

FIGURE 7. The scanning region is highlighted. Two scale gradations were used of; 5*cm* × 2*cm* for larger maps of the defect, and 1*cm* × 1*cm* of each defect individually and the local area around them. The cross-cutting dotted guides indicate the approximate positions and boundaries of the internal stiffener bonds holding the non-structural foam core in-between as seen in Fig: 5 and Fig: 6.

composite material, reducing the efficacy of machine learning methods using raw depth information.

A cross sectional schematic of the defects with internal features are shown in Fig: 8.

IV. EXPERIMENTAL RESULTS

Several scans of a Class Severn hull boat were performed, collecting force and sound data with the hand-held EVOTIS device seen in Fig: 9, using stencilled guides to ensure repeatability and accurate relative positioning. A C-scan representation is reconstructed by recording the position of each specific A-scan taken within the grid. The tool was held flat against the surface using the square aperture to prevent skewing of the striking hammer from the surface. Though tool-offset error is minimised so that the striking force is consistent, human positioning error is present as the operator misaligns the tool with the provided stencil. The data was then visualised in Python, with a logarithmic energy scale as it better highlights changes in depth. All results in this section are plotted with x and y axes in units of cm.

The experimental set-up involved the EVOTIS TT device manually applied over a grid-stencilled part, and the data collected on an external computer, shown in Fig: 10.

The logarithmic values of sonic response functions described in Eq: 2 and Eq: 8 were seen to provide greater imaging clarity. For these reasons, the units of sound are used for imaging are $\log(mV)$. While prior information analyses would indicate the local and global modes, the purpose of this paper is to present application to an unknown part. The EVOTIS device is calibrated to ensure that it can identify the back-wall of the triangular wedge and the thinnest portion of GFRP skin only, providing a realistic scenario in which on-site access to the part is limited and defect depth unknown.

A. FORCE AND SOUND RESPONSES

Though the defect-stiffness approach is validated for similar components to those considered here by [19], contact time results are experimentally found to be insufficient in this use-case, an example of which is shown in Fig: 11.

The sonic response method is the primary candidate for defect detection. The prior full energy spectrum is compared with both matrix trace and metric function q in their ability to produce consistent, noise-free depth imaging of parts and in the identification of defects.

B. MODAL CONVERSION

Conversion of energy from local to global modes can be seen in Fig: 12. This data is collected from the full sample region shown in Fig: 7, and varying time sampling windows are taken in order to confirm modal spread from the local to global. Since the metric value q is independent of total sonic energy, it measures the distribution of sonic energy in the binary bins of local and global modes. The observed half-sinusoidal contact period is $T = 0.14ms$, and time windows t are taken in proportion to this time period. The data shows that global modes absorb the majority of energy within one half-period of the contact motion. When the sampling window is increased to the full sinusoidal period of $0.28ms$ labeled as $t/T = 1$, the energy absorbed by global modes increases from 70% to 90% of the total sonic energy emitted by the surface, confirming the presence of modal spread while also confirming that there is significant initial resonance between the instrumented impact and global modes.

The effect on imaging for matrix trace and full energy methods is also investigated. The same region is imaged with both methods, presented in Fig: 13.

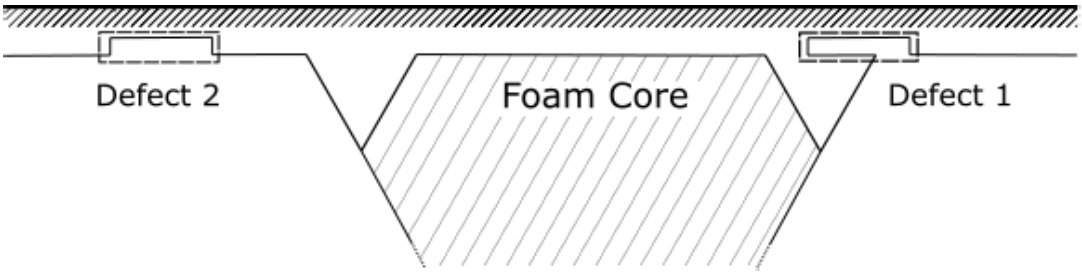

FIGURE 8. Cross section of the surface shown from the front in Fig: 7, outlining the structural features seen in Fig: 6.

FIGURE 9. EVOTIS Instrumented Tap Testing device features a square faced contact aperture to ensure the strike is normal to the surface, consistent force application, and collects both force and sound time histories.

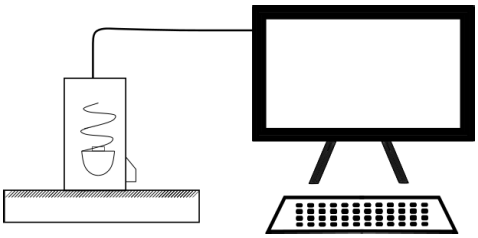

FIGURE 10. Experimental set-up of the TT device connected to an external computer. Data from the device was loaded into the EVOTIS software, then saved in csv format.

The traditional energy method shows the defects most clearly within one half-period of the sinusoidal motion, reflecting the local modalities most clearly. Meanwhile, the matrix trace method produces images better reflecting the underlying smooth depth variations with greater time sampling windows. However, imaging with the full energy spread provides clearer indications of the defects. If the underlying structure is known, the full energy method would provide a clearer map of defects. However several false positives may be identified with variations in signal strength, mos clearly seen in-between triangular wedges where in lieu of a detailed part schematic, it is deduced that the composite skin is of marginally reduced thickness. Cost function q is used to identify depth variations with greater clarity using the energetic spread of modal energy, the mapped results of which can be seen in Fig: 14.

In all sampling regimes the defects can be clearly identified as peaks of the modal conversion metric. As observed in Fig: 12, modal spread increases with time, initially focused around the defective regions and later highlights regions of depth variation around the triangular wedges. These results imply that for defective regions where there is a sudden change in depth, the global modes resonate with the instrumented tap far more than the local modes, and that the energy induced in local modes of excitation is dispersed into global modes over the surface, particularly in regions where there is depth variation such as at the wedge boundary points.

The image quality for each metric differs in optimal sampling window. The traditional full energy metric is optimised for a sampling time over just the contact period, highlighting the defective regions with fewer peaks elsewhere in the domain. Imaging in this domain results in granularity and identical signal response between the thinner non-defective region surrounding the bonding wedges, and the thinner defective region cutting through the wedge agreeing with the signal response schematic given in Fig: 8 that invalidates use of machine learning or spectral filtering techniques used elsewhere in the literature. The matrix trace method provides an optimal map of the structural features with a greater time sampling regime, allowing the operator to localise the scan with reference to features either with prior knowledge of the part or in accumulating an image of the part iteratively. In any sampling regime its utility in identification of defects is at best equal to the traditional full energy method, however, highlighting its utility in accurately identifying structural features only. However for the metric q, defects are best recognised in the half-period time sampling regime, with secondary features such as local wedge depth variation becoming pronounced with an increased sampling window.

V. DEFECT IDENTIFICATION

Utilising the results of the previous section, the defects and structural features are imaged in greater clarity with the use of optimal sampling conditions, and are compared with the full-energy method. Both defective regions are re-scanned with a spatial resolution of $1cm \times 1cm$. Defect one is imaged in Fig: 15 and defect two in Fig: 16. As seen in Fig: 15, the defective area cannot be clearly seen with either full energy or matrix trace imaging methods. However the structural

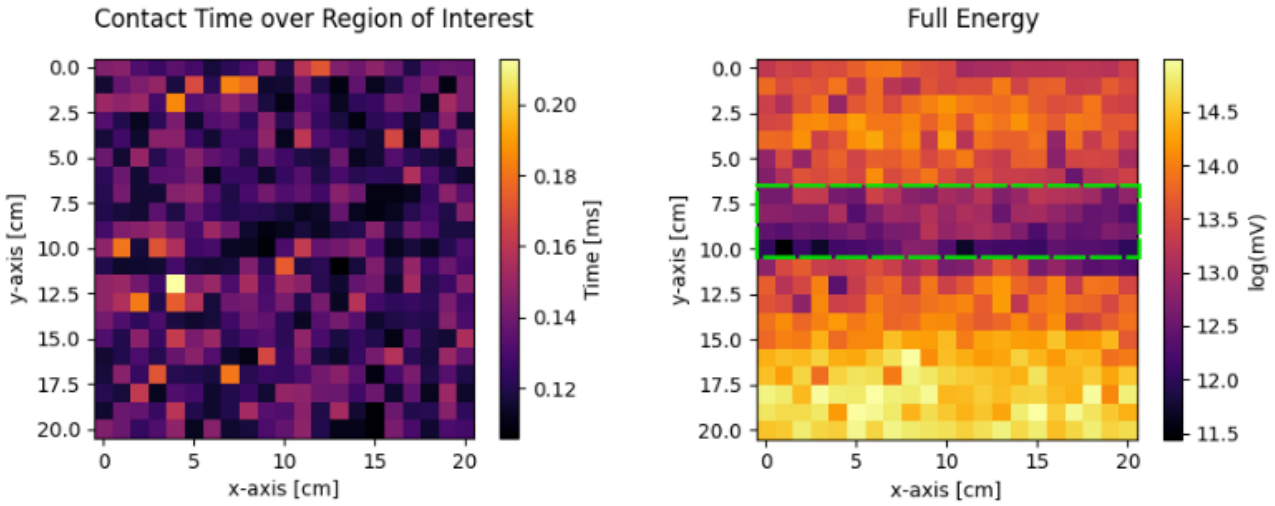

FIGURE 11. Contact time vs Full Energy imaging of a non-defective region. This scan is taken with the triangular stiffener bond section as seen in Fig: 5 and whose position is highlighted in Fig: 7 aligned to the x-axis, the variation in depth of the bond section shown in the variations of the sonic response, bounded by the green lines 4*cm* apart. Contact time undergoes little fluctuation, the results are constituted mainly of noise. The comparison imaging method shows depth fluctuations by using Eq: 2, highlighting the need for sonic rather than force based imaging methods.

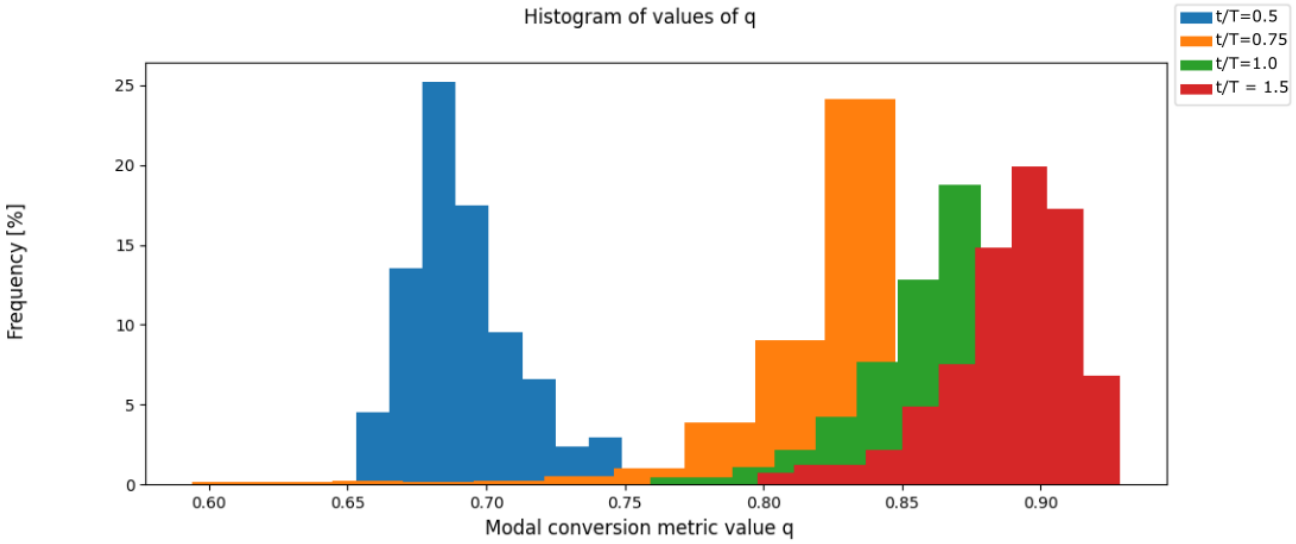

FIGURE 12. The metric value *q* describes the proportion of observed energy absorbed by global resonance modes. While after one half-period of the sinusoidal contact motion 70% of observed audible energy is absorbed by global modes, this increased to 85% within a full contact-period. This sample is from a defect-free cross section including a stiffener bond.

features are seen with greater clarity using the matrix trace method. The metric q highlights the defect clearly in the half-period regime and the wedges edges, highlighted with vertical white lines, are present in the full period regime.

When a smoothing filter is applied over the half-period samples of the metric q, the defects become significantly clearer. The smoothing window reduces noise within the metric, highlighting the spatially significant distribution of higher values of q that correlate with the presence of defects. In this use-case defects larger than $10cm \times 10cm$ are considered critical, and so a $5cm \times 5cm$ average smoothing window provides accurate results for this aim. Applying such a window, it is shown with the novel metric introduced that an operator could easily identify defective regions where in the full-energy imaging method used for the sonic response, the operator would struggle to determine true positives when testing the sample for defects and also in not identifying false positives.

Images showing greater structural clarity with the matrix trace method, and the location of both defects with the metric q values is displayed in Fig: 17.

This process is also validated on the sampling regimes of $1cm \times 1cm$, shown in Fig: 18 where both the underlying structure and defects can be identified with ease.

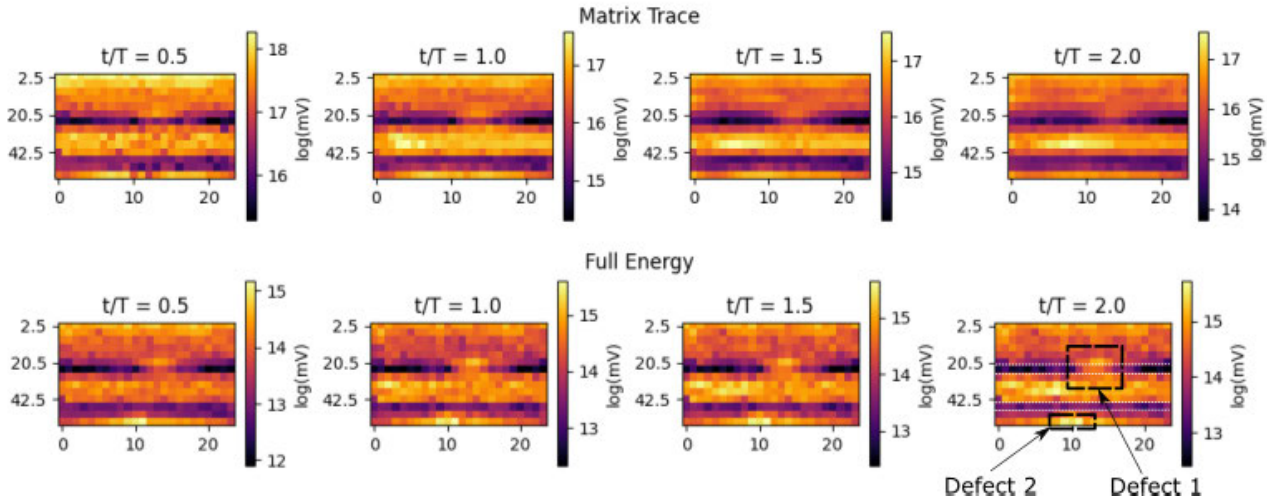

FIGURE 13. Comparison of the matrix trace and full energy methods of defect imaging within different time windows. The full energy method provides less consistent depth measurement results than the matrix trace method at higher sampling times. Axis values are in cm.

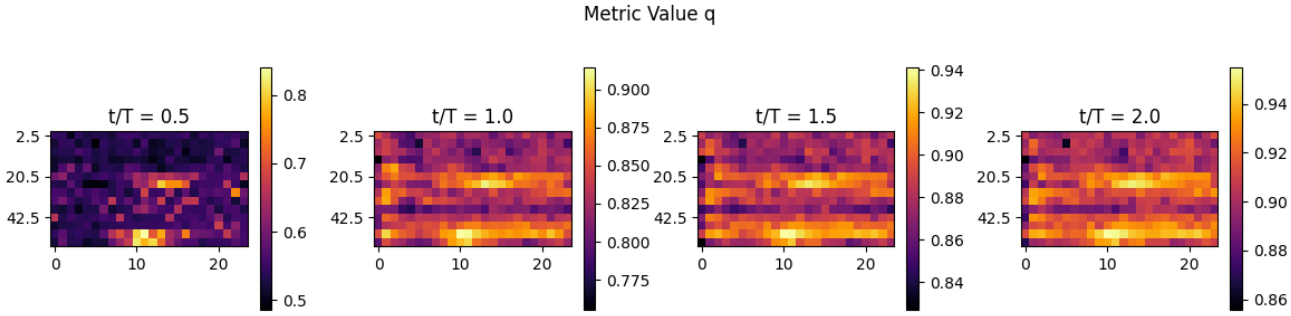

FIGURE 14. Metric function *q* highlights the divergence of surface excitations from local to global modes with an increased time window. Axis values are in *cm*, q is a dimensionless quantity.

VI. DISCUSSION

This paper sought to identify an effective use of data in identifying defects within curved lifeboat hulls for which there is no digital twin of the structure containing thickness or precise material information. The method used is to be suitable for an automated robotised inspection system for future deployment, involving a robotic arm equipped with a mobile base.

The thickness of the sample part meant force data was unsuitable, while the traditional metric of measuring the sound response did not provide a map with great enough clarity for an operator to accurately identify defects with minimal prior knowledge of the structure of the part. This could in a realistic dock scenario result in time lost for the vessel to unnecessary maintenance of non-defective regions. The cause of this was found to be the interference of global modes of resonance being excited and exhibited in the scanning procedure, as is suggested by the advanced literature on Tap Testing. The robotised deployment aspect removed the possibility of using physical solutions such as sound baffles for audio isolation since these would present additional risks such as snagging negative their potential for automatic deployment.

Building upon results used in he area of Force Reconstructions, the matrix trace method was introduced to give the operator greater clarity of the underlying part structure. While the matrix trace method did not provide adequate indications of defects, the improved reliability of response to different surface depths will allow future work to consider this data as a source of reconstruction algorithms. These future works will seek to produce accurate digital twins and data reconstructions in the case of mobile robotic deployment where the base's odometric readings have a relatively high margin of error, in a similar way to point cloud reconstructions.

To provide accurate defect identification the metric q was introduced, measuring surface depth variations through the relative spread of global and local energetic modes. This metric proved that the modal spread from local resonant modes of interest to global interference modes does occur. With a smoothing window applied, it was further shown the defects could be easily identified, even when the surface depth variation was modest and the depth of the defect differed

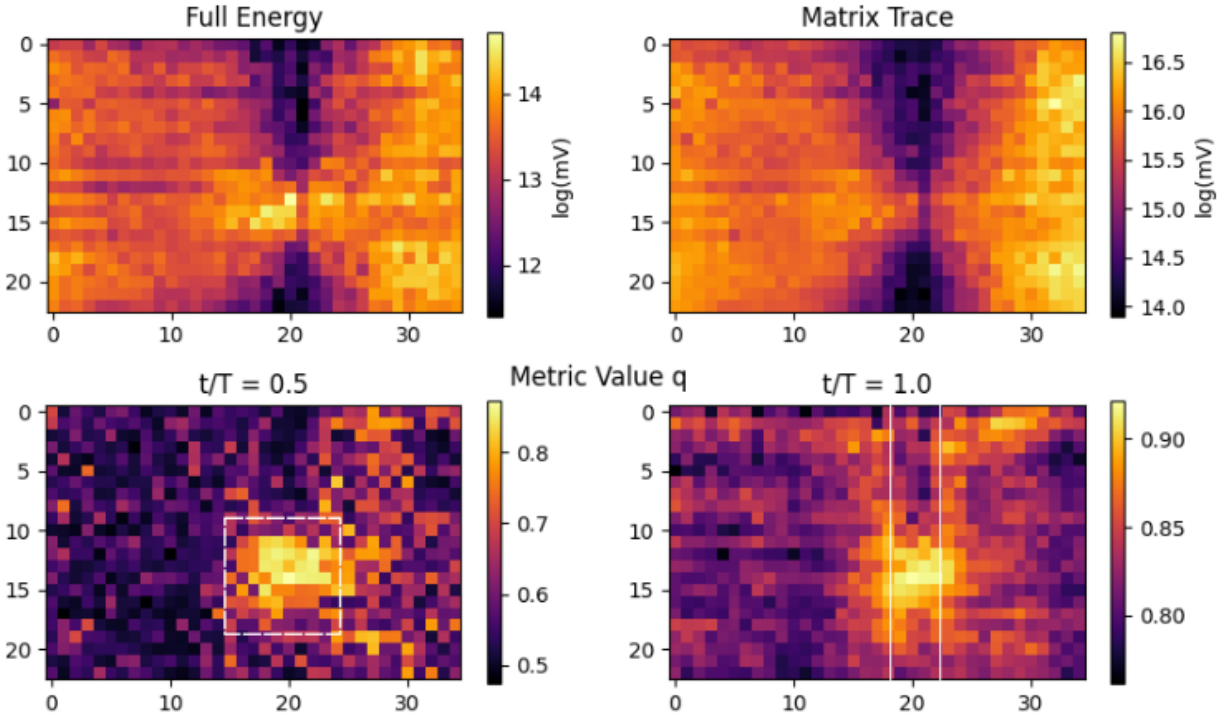

FIGURE 15. Imaging of defect one. Metric value *q* taken across two sampling regimes shows the defective region highlighted in the first sampling regime, the 10*cm* × 10*cm* bounds of which are highlighted. The boundaries of the 4*cm* wide cross-cutting wedge bond are overlaid in white in the full period sampling regime, and are seen as positions of depth flux with the *q* metric. Axis values are in *cm*. This scan was taken with the wedge aligned to the y-axis. Both full energy imaging and matrix trace imaging were completed in the half-period time sampling regime, as the results earlier indicated this sampling period provided greater clarity in results.

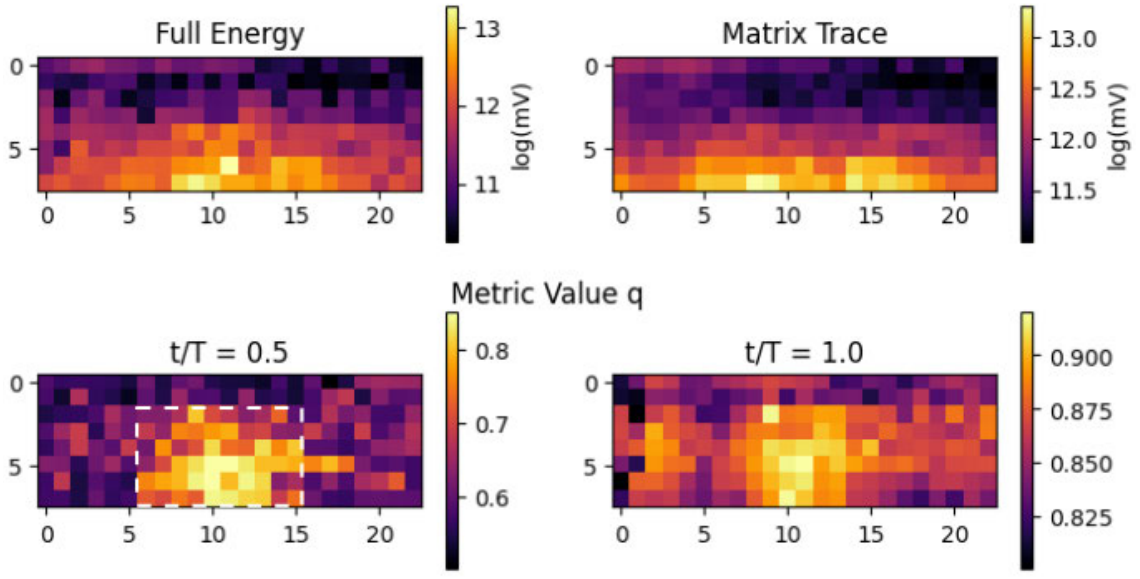

FIGURE 16. Imaging of the second defective region. There are no structural features surrounding the defect, resulting in a smoother map for the second sampling regime. The top 3/4 of the defect were imaged, since a strap holding the part in place seen in Fig: 7 prevented access to the remainder of the defect. Despite the smaller depth differential between the defect and its surroundings, the defect highlighted with a white box can still be clearly identified. Axis values are in *cm*. Both full energy imaging and matrix trace imaging were completed in the half-period time sampling regime.

little from surrounding non-defective regions in the case of defect one.

In cases where prior information can be incorporated, accurate calibration and filtering of signal response can be used

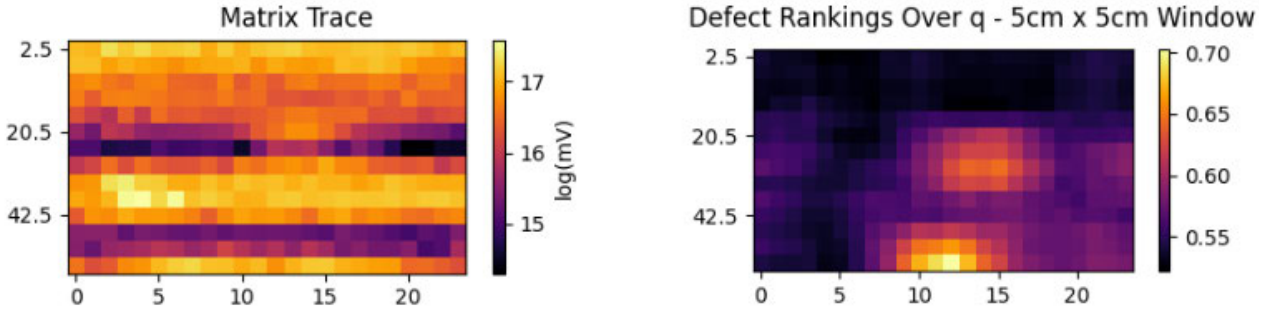

FIGURE 17. Both defects are clearly highlighted when the values of q are smoothed by a rolling averaging window when compared to the sonic method presented in Fig: 13, despite having difference depths and different depth differentials with the surrounding surface. Axis values are in *cm*. Both full energy imaging and matrix trace imaging were completed in the half-period time sampling regime.

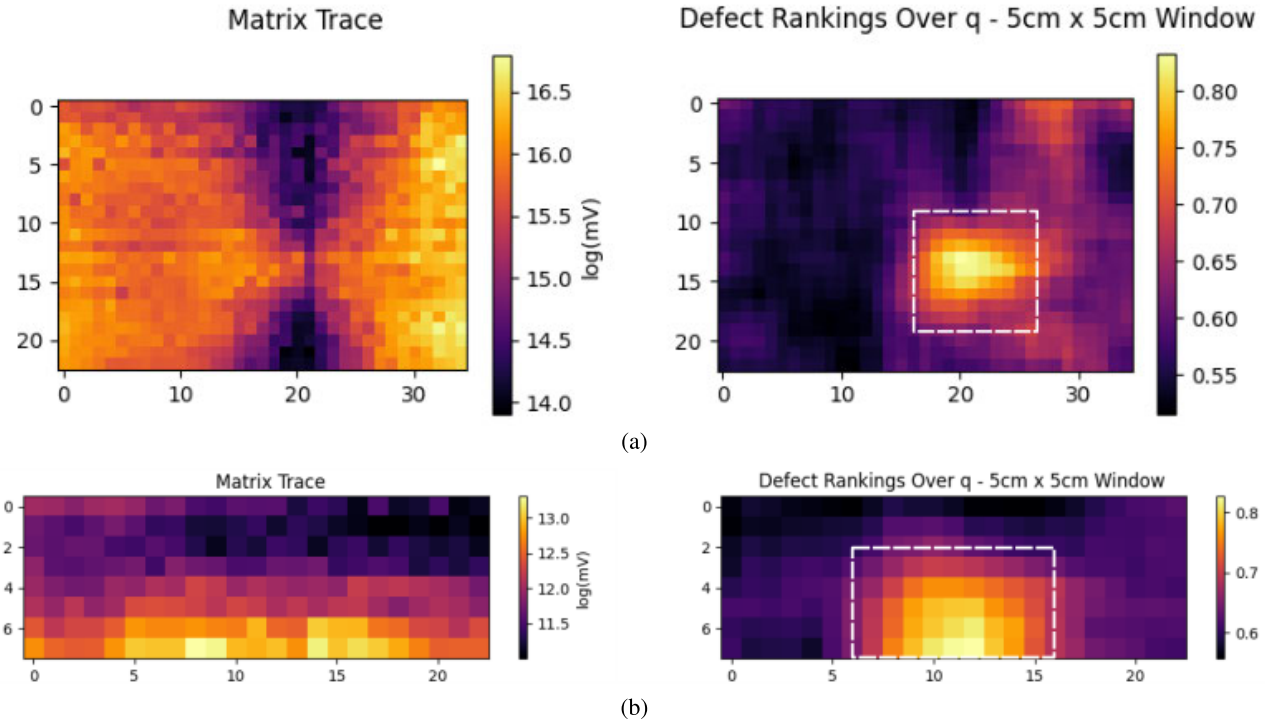

FIGURE 18. Matrix trace method is used to detect the underlying structure of the part, and metric q identifies defects. 18a The first defective region, with cross-cutting bond wedge is shown. 18b The second defective region is imaged. For both defects, the smoothing window applied to the half-period sampled data shows clearly where the defects are. Axis values are in *cm*. Defects are highlighted. Both full energy imaging and matrix trace imaging were completed in the half-period time sampling regime.

as a way of identifying defective regions and so remove the need for force data entirely. Further, the device would need to be calibrated for thicker and stiffer materials to ensure the induction of resonant material modes, making prior material knowledge preferable in order to reduce scanning times. In instances of high through-put or parts equipped with digital twins, the presented methods may be sub-optimal to those using prior knowledge. Further, these methods are to be tested on a wider range of materials to validate them for components beyond thick GFRP sections.

ACKNOWLEDGMENT

Materials used in this project were procured as part of an initiative known as the Advanced Engineering Materials Research Institute (AEMRI).

REFERENCES

[1] W. Goldsmith and J. T. Frasier, "Impact: The theory and physical behavior of colliding solids," *J. Appl. Mech.*, vol. 28, no. 4, p. 639, Dec. 1961.

[2] P. Cawley and R. D. Adams, "The mechanics of the coin-tap method of non-destructive testing," *J. Sound Vib.*, vol. 122, no. 2, pp. 299–316, Apr. 1988.

[3] J. J. Peters, D. J. Barnard, N. A. Hudelson, T. S. Simpson, and D. K. Hsu, "A prototype tap test imaging system: Initial field test results," *AIP Conf. Proc.*, vol. 509, pp. 2053–2060, May 2000.

[4] R. Schroeer, "The acoustic impact technique," *Non-Destructive Test.*, vol. 3, no. 3, pp. 194–196, Jun. 1970.

[5] P. Cawley and R. D. Adams, "Sensitivity of the coin-tap method of nondestructive testing," *Mater. Eval.*, vol. 47, no. 5, pp. 558–563, 1989.

[6] Y. Li, J. Zhang, J. Zhao, and J. Hu, "Research on intelligent tap testing of aviation composite material," in *Proc. Int. Conf. Adv. Mater. Sci. Environ. Eng.* Amsterdam, The Netherlands: Atlantis Press, 2016, pp. 44–47.

[7] P. Cawley, "A high frequency coin-tap method of non-destructive testing," *Mech. Syst. Signal Process.*, vol. 5, no. 1, pp. 1–11, Jan. 1991.

[8] P. Cawley and C. Theodorakopoulos, "The membrane resonance method of non-destructive testing," *J. Sound Vib.*, vol. 130, no. 2, pp. 299–311, Apr. 1989.
[9] W. M. Hartmann and J. V. Candy, "Acoustic signal processing," in *Springer Handbook of Acoustics*, T. D. Rossing, Eds. New York, NY, USA: Springer, 2014, pp. 519–563.
[10] R. I. Mackie and A. E. Vardy, "Applying the coin-tap test to adhesives in civil engineering: A numerical study," *Int. J. Adhes. Adhesives*, vol. 10, no. 3, pp. 215–220, Jul. 1990.
[11] S. Esola, I. Bartoli, S. E. Horner, J. Q. Zheng, and A. Kontsos, "Defect detection via instrumented impact in thick-sectioned laminate composites," *J. Nondestruct. Eval.*, vol. 36, no. 3, Sep. 2017, Art. no. 47.
[12] W. Huadong and M. Siegel, "Correlation of accelerometer and microphone data in the 'coin tap test,'" *IEEE Trans. Instrum. Meas.*, vol. 49, no. 3, pp. 493–497, Jun. 2000.
[13] J. C. S. Queiroz, Y. T. B. Santos, I. C. da Silva, and C. T. T. Farias, "Damage detection in composite materials using tap test technique and neural networks," *J. Nondestruct. Eval.*, vol. 40, no. 1, Mar. 2021, Art. no. 27.
[14] E. Jacquelin, A. Bennani, and P. Hamelin, "Force reconstruction: Analysis and regularization of a deconvolution problem," *J. Sound Vib.*, vol. 265, no. 1, pp. 81–107, Jul. 2003.
[15] M. E. De Simone, F. Ciampa, and M. Meo, "A hierarchical method for the impact force reconstruction in composite structures," *Smart Mater. Struct.*, vol. 28, no. 8, Aug. 2019, Art. no. 085022.
[16] M. Thiene, Z. Sharif-Khodaei, and M. H. Aliabadi, "Comparison of artificial neural networks and the transfer function method for force reconstruction in curved composite plates," in *Key Engineering Materials*, vol. 627. Zürich, Switzerland: Trans Tech Publications, Sep. 2014, pp. 301–304.
[17] M. Thiene, M. Ghajari, U. Galvanetto, and M. H. Aliabadi, "Effects of the transfer function evaluation on the impact force reconstruction with application to composite panels," *Compos. Struct.*, vol. 114, pp. 1–9, Aug. 2014.
[18] S. J. Kim, "Damage detection in composite under in-plane load using tap test," *J. Mech. Sci. Technol.*, vol. 29, no. 1, pp. 199–207, Jan. 2015.
[19] D. K. Hsu, D. J. Barnard, J. J. Peters, and V. Dayal, "Physical basis of tap test as a quantitative imaging tool for composite structures on aircraft," *AIP Conf. Proc.*, vol. 509, pp. 1857–1864, May 2000.

ALASTAIR POOLE received the master's degree in mathematics from Durham University, in 2018. He is currently pursuing the Ph.D. degree in robotic non-destructive testing with the University of Strathclyde in partnership with The Welding Institute Wales. His research interests include enabling robotic non-destructive testing in unstructured environments and applied mathematical physics for enhanced sensing.

NATHAN HARTLEY is an experienced Chartered Engineer and the Project Manager with more than 20 years experience in the defense, nuclear, energy, manufacturing, and non-destructive testing industries. Since 2018, he has been with The Welding Institute (TWI), where he managed a variety of complex and high-value engineering and research projects with a focus on automation and development of novel NDT techniques. He recently introduced multi-frequency microwave inspection to TWI's capabilities and has been instrumental in the integration and use of mobile and collaborative robots. He has also overseen the development of a novel, automated acoustic inspection method for the inspection of highly attenuative glass fibre structures. He is an accomplished NDT practitioner, holding CSWIP Level II qualifications in UT and PAUT (Welds).